molecule in this site. The Cu^{2+} remains in this cavity as the dehydration temperature is raised, becoming irreversibly trapped in the cavity at dehydration temperatures above 150–200 °C.

Acknowledgment. This research was supported by the Texas Advanced Technology Research Program and the R.A. Welch Foundation.

Registry No. Cu^{2+}, 15158-11-9; Mg^{2+}, 22537-22-0; montmorillonite, 1318-93-0.

Theoretical and ESR/ENDOR Single-Crystal Study of an Azaallyl Radical

Malledi V. V. S. Reddy,[†] Alice Celalyan-Berthier,[†] Michel Geoffroy,*[†] Pierre Y. Morgantini,[‡] Jacques Weber,[‡] and Gerald Bernardinelli[§]

Contribution from the Department of Chemistry, University of Geneva, 1211 Geneva 4, Switzerland. *Received June 12, 1987*

Abstract: The room-temperature-stable radical trapped in an X-irradiated single crystal of 2-bromo-5-nitrothiazole has been studied by ^1H ENDOR and by ESR. The structure of the undamaged crystal has been determined. The **g** tensor, the magnetic hyperfine tensors with ^1H, ^{79}Br, ^{81}Br, and the quadrupolar interaction tensors with ^{79}Br and ^{81}Br have been obtained and their orientations are compared with the bond directions of the original molecule. They lead to the identification of an azaallyl radical R(H)C–N–C(Br)R and give experimental information about the spin delocalization in the C–N–C moiety. The ab initio optimized geometries of CH_2–N–CH_2 and of CH_2–N–CHX (where X = Cl, Br) have been calculated. The theoretical spin densities are obtained together with the calculated magnetic and quadrupolar hyperfine tensors. Experimental results are shown to agree with the theoretical predictions. The possibility of delocalization induced by incorporation of the radical in a thiazolidine ring is also investigated. Allyl and azaallyl structures are compared.

Allyl-type radicals present considerable interest in theoretical and organic chemistry;[1-6] $(C_3H_5)^\bullet$ is indeed the simplest odd-alternate hydrocarbon exhibiting negative spin density on a carbon atom, and allyl derivatives frequently appear as reaction intermediates in heterocyclic chemistry. Curiously, although particular attention has been recently paid to cationic allyl homologues[7-9] containing one or more heteroatoms (e.g., R_2C–O–$CH_2^{\bullet+}$, R_2C–NH–$CR_2^{\bullet+}$), the simple azaallyl radical, H_2C–N–CH_2, is considerably less known. It has principally been observed in solution after substitution of the hydrogen atoms by bulky diphenylene groups.[10-11] The results of Grossi et al.,[12] who showed that an azaallylic radical can be created in solution by photolysis of 2-methylthiazoline, together with our recent finding[13] on the trapping of an allyl radical in crystalline nitrothiophene, prompted us to try to generate an azaallylic species in a single crystal of a thiazole derivative. Trapping of this radical in a single-crystal matrix should, indeed, provide the most suitable information for a comparison with quantum chemical calculations.

In the present study, we show that the bromoazaallyl radical **1** can be generated by X-irradiation of a single crystal of bromonitrothiazole **2**. The ESR and ENDOR studies, together with the crystal structure of the undamaged molecule, provide a detailed description of this azaallyl species. Theoretical information is obtained from ab initio calculations performed on the azaallyl radical and some of its derivatives. After optimization of the geometries and calculation of the spin densities, a theoretical estimation of the magnetic and quadrupolar hyperfine interactions

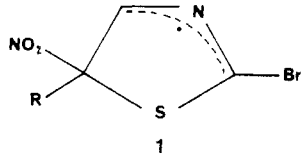

1

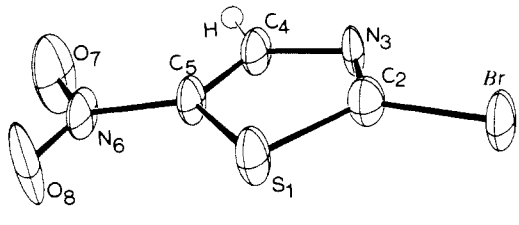

2

Table I. Fractional Coordinates and Equivalent Isotropic Temperature Factors, U_{eq} ($Å^2 \times 10^3$)[a]

	X	Y	Z	U_{eq}
Br	0.5919 (4)	0.25	0.9068 (3)	43.4 (11)
S(1)	0.7147 (7)	0.25	0.6013 (8)	41 (3)
C(2)	0.575 (3)	0.25	0.708 (3)	36 (9)
N(3)	0.4587 (22)	0.25	0.6439 (22)	33 (8)
C(4)	0.478 (3)	0.25	0.500 (3)	35 (10)
C(5)	0.607 (3)	0.25	0.4586 (23)	31 (9)
N(6)	0.658 (3)	0.25	0.3158 (21)	37 (8)
O(7)	0.5734 (25)	0.25	0.2223 (21)	77 (11)
O(8)	0.7765 (20)	0.25	0.2985 (23)	71 (11)
H(4)	0.3945	0.25	0.4230	51

[a] Esd's are in parentheses. U_{eq} is the average of the eigenvalues of U.

[†] Department of Physical Chemistry.
[‡] Laboratoire de Chimie Théorique Appliquée.
[§] Laboratoire de Cristallographie aux Rayons X.

(1) (a) Heller, C.; Cole, T. *J. Chem. Phys.* **1962**, *37*, 243. (b) Fessenden, R. W.; Schuler, R. H. *Ibid.* **1963**, *39*, 2147.
(2) Takada, T.; Dupuis, M. *J. Am. Chem. Soc.* **1983**, *105*, 1713.
(3) Feller, D.; Davidson, E. R.; Borden, W. T. *J. Am. Chem. Soc.* **1984**, *106*, 2513.
(4) Korth, H. G.; Lomnes, P.; Sustmann, R. *J. Am. Chem. Soc.* **1984**, *106*, 663.
(5) Baird, N. C.; Gupta, R. R.; Taylor, K. F. *J. Am. Chem. Soc.* **1979**, *101*, 4531.
(6) Walton, J. C. *Rev. Chem. Intermed.* **1984**, *5*, 249.
(7) Qin, X. Z.; Williams, F. *J. Phys. Chem.* **1986**, *90*, 2292.
(8) Qin, X. Z.; Snow, L. D.; Williams, F. *J. Am. Chem. Soc.* **1985**, *107*, 3366.
(9) (a) Kispert, L. D.; Pittman, C. U.; Lee Allison, D.; Patterson, T. B.; Gilbert, C. W.; Hains, C. F.; Prather, J. *J. Am. Chem. Soc.* **1972**, *94*, 5979. (b) Lien, M. H.; Hopkinson, A. C. *Can. J. Chem.* **1984**, *62*, 922.
(10) Kuhn, R.; Neugebauer, F. A. *Monatsh. Chem.* **1963**, *94*, 1.
(11) Watanabe, K. *Bull. Chem. Soc. Jpn.* **1975**, *48*, 1732.
(12) Grossi, L.; Lunazzi, L.; Placenti, G. *Tetrahedron Lett.* **1981**, *22*, 251.
(13) Geoffroy, M.; Celalyan-Berthier, A.; Reddy, M. V. V. S.; Bernardinelli, G.; Papadopoulos, M. *J. Chem. Phys.* **1985**, *82*, 4850.

0002-7863/88/1510-2748$01.50/0

is performed, which enables a comparison with the experimental values. The structural modifications induced by the substitution of the central allyl carbon by a nitrogen atom are investigated as well as the possibility of spin delocalization resulting from the incorporation of the radical into a thiazolidine ring.

Experimental Section

Compounds. Bromonitrothiazole is a commercial compound (EGA Chemie) purified by recrystallization from benzene. The single crystals have been obtained by slow evaporation of a solution in this solvent; the irradiation has been performed at 77 K and at room temperature by using a Philips X-ray tube with a tungsten anticathode.

Crystallographic Data. A single crystal of $C_3HN_2O_2SBr$ (MW 209.0, average dimension 0.13 × 0.32 × 0.38 mm) was sealed in a Lindemann capillary under Ar. The lattice parameters and intensities have been measured at room temperature on a Philips PW1100 diffractometer with a graphite monochromated Mo Kα radiation (λ = 0.71069 Å): orthorhombic, *Pnma*, a = 10.0323 (10), b = 6.4596 (8), c = 9.3342 (8) Å; V = 604.9 Å; Z = 4; D_c = 2.295 g cm^{-3}; μ = 6.98 mm^{-1}; $F(000)$ = 400; cell dimensions from 23 reflections (2θ = 33–40°); data collection: sin $\theta/\lambda < 0.62$; $\omega/2\theta$ scans, ω-scan angle 1.4°, absorption correction by Gaussian grid integration on grid of 6 × 6 × 6 points, $2.35 \le A^* \le 7.61$; two standard reflections showing a loss of about 18% of the peak intensities during the collection (all the reflections are corrected for this drift), 652 independent reflections, 411 observed reflections with $|F| \ge 4\sigma(F)$ and $|F| \ge 8$; distribution of data $\langle E^2 - 1 \rangle$ = 1.168 indicated centrosymmetric space group. The structure has been solved by direct methods (MULTAN 80[14]) and refined by full-matrix least-squares (55 parameters) using $|F|$ values; there is no secondary-extinction correction; the coordinates of the hydrogen atom have been calculated: $R = wR = 0.071$ (w = 1). Atomic scattering factors and anomalous dispersion terms for Br, S, N, and O atoms have been taken from the *International Tables for X-Ray Crystallography*.[15] All calculations have been performed with a local version of XRAY76[16] and ORTEPII.[17] The positional parameters and equivalent isotropic temperature factors are given in Table I.

Instrumentation. The ESR spectra have been recorded on a Bruker 200 D spectrometer (X-band, 100-kHz field modulation). Some spectra have also been recorded on a Varian E-9 spectrometer equipped with a cavity which allows the precise orientation of the crystal in any given direction with respect to the static magnetic field.[18] The ENDOR spectra have been obtained on a Varian spectrometer equipped with a homemade ENDOR device.[19] The angular dependence of the ESR/ENDOR spectra has been studied by rotating the crystal around the crystallographic axes and by recording the spectra every 10°.

ESR Analysis. The ESR spectra have been analyzed by using the following Hamiltonian:

$$\mathcal{H} = \beta HSgh + S(^1\mathrm{H})\mathbf{T}I + S(^{79/81}\mathrm{Br})\mathbf{T}I + I(^{79/81}\mathrm{Br})\mathbf{P}I$$

where **T** corresponds to the magnetic hyperfine coupling tensor and **P** to the quadrupolar hyperfine tensor.

When quadrupolar and magnetic interactions are similar in magnitude, the most intense lines of the ESR spectra are often $\Delta M_I = \pm 1, \pm 2$ transitions;[20] in this case the spectra can be analyzed only by adjusting the **g** and the magnetic and quadrupolar hyperfine tensors to fit the experimental spectra. This adjustment has been performed by using a seventh-order perturbation program[21] which calculates the position and the intensity of allowed and forbidden transitions. This adjustment is facilitated by the presence of two isotopes (^{79}Br and ^{81}Br), whose natural abundance, magnetic moments, and quadrupolar moments are known (^{79}Br: g_n = 1.3993; natural abundance: 50.5%, $Q = 0.33|e|10^{-24}$; ^{81}Br: g_n = 1.5084, natural abundance 49.5%, $Q = 0.28|e|10^{-24}$). The resulting tensors are considered to be satisfactory when they allow one to simulate the ESR spectrum obtained for any given orientation of the magnetic field. For all the orientations an additional coupling with a ^{14}N nucleus has been needed to get the final spectrum. A Gaussian line shape has been used for these simulations.

Calculations. The computations have been performed on a VAX 8700 computer. GAUSSIAN 80 and 82 versions[22] have been used for ab initio calculations. The optimized geometries for $H_2C\dot{-}CH-CH_2$, $H_2C\dot{-}N-CH_2$, $H_2C\dot{-}N-CHCl$, and $H_2C\dot{-}N-CHBr$ have been obtained from UHF calculations by using the gradient optimization technique.[23,24] Hartree–Fock SCF calculations have been carried out with the 6-31G* basis set for all the acyclic radicals except for $CH_2\dot{-}N-CHBr$ for which we have used, for bromine, the basis set reported by Mezey et al.[25] The 4-31G* basis set has been used for the cyclic radicals. Spin contamination of the UHF wave function due to quartet component has been annihilated through the projection operator technique suggested by Amos and Snyder,[26a] as implemented in the GAUSSIAN 80 program by Cremaschi et al.[26b]

In the LCAO approximation, the Fermi contact contribution to the magnetic hyperfine interaction at nucleus N is given by:[27]

$$A^{\mathrm{N}}_{\mathrm{iso}} = (8\pi/3)g_e\beta_e g_n\beta_n|\Psi_{\mathrm{N}}(0)|^2$$

where

$$|\Psi_{\mathrm{N}}(0)|^2 = \sum_{\mu,\nu} P^{\alpha-\beta}_{\mu\nu}(\phi_\mu|\delta(r_{\mathrm{N}})|\phi_\nu\rangle$$

$P^{\alpha-\beta}_{\mu\nu}$ being the first-order UHF spin-density matrix. On the other hand, the components of the electric field gradient at nucleus N are given by:

$$q^{\mathrm{N}}_{uv} = e\sum_{\mathrm{K}\neq\mathrm{N}}\{Z_{\mathrm{K}}[3(u_{\mathrm{K}} - u_{\mathrm{N}})(v_{\mathrm{K}} - v_{\mathrm{N}}) - R^2_{\mathrm{KN}}\delta_{uv}]/R^5_{\mathrm{KN}}\} - e\sum_{\mu,\nu} P_{\mu\nu}(\phi_\mu|(3uv - r^2\delta_{uv})/r^5|\phi_\nu\rangle$$

where u, v represent x, y, z; the first summation runs over the nuclei, with atomic numbers Z_{K} and coordinates x_{K}, y_{K}, z_{K}, of the molecule, R_{KN} is the distance between nuclei K and N. $P_{\mu\nu}$ is the total (i.e., $\alpha + \beta$) first-order density matrix and r is the distance between the electron and nucleus N. The q^{N}_{uv} tensor components, which lead to the nuclear quadrupole tensor elements $e^2Qq^{\mathrm{N}}_{uv}$, are directly related to the ESR (N)**P** tensor through the expression:

$$(\mathrm{N})P_{uv} = e^2Qq^{\mathrm{N}}_{uv}/2I(2I - 1)$$

where I is the spin at nucleus N.

In this study, both $A^{\mathrm{N}}_{\mathrm{iso}}$ and q^{N}_{uv} components have been evaluated by adapting part of the POLYATOM program[28] to the GAUSSIAN 80 code.

Results

ESR and ENDOR Spectroscopies. The ESR/ENDOR reference frame has been chosen to coincide with the crystallographic axes ($x//a, y//b, z//c$). The crystal structure (Table I) shows that the bromonitrothiazole molecule is localized in a special position on the mirror plane perpendicular to the crystallographic b axis. The C–Br bond direction is almost aligned along the c direction ($\angle$C–Br,c axis = 5°).

X-irradiation at 77 K leads to an intense ESR spectrum exhibiting weak half-field transitions (forbidden $\Delta M_s = \pm 2$ transitions) which disappear near 170 K. The $g \simeq 2$ region of the spectrum is also temperature dependent and a well-resolved spectrum is observed above 230 K (Figure 1). The high-temperature spectra can be directly obtained by X-irradiation at 298 K; they are due to a radical stable at room temperature, which

(14) Main, P.; Fiske, S. J.; Hull, S. E.; Lessinger, L.; Germain, G.; Declercq, J. P.; Woolfson, M. M. "A System of Computer Programs for the Automatic Solution of Crystal Structures from X-Ray Diffraction Data"; University of York, England and Louvain-la-Neuve, Belgium, 1980.
(15) *International Tables for X-Ray Crystallography*; Kynoch Press: Birmingham, 1974; Vol. IV.
(16) Stewart, J. M.; Machin, P. A.; Dickinson, C. W.; Ammon, H. L.; Heck, H.; Flack, H. (976). "The X-Ray'76 System"; Technical Report TR 446; Computer Science Center, University of Maryland: College Park, MD.
(17) Johnson, C. K. ORTEPII. Report ORNL-5138; Oak Ridge National Laboratory: Oak Ridge, TN, 1976.
(18) Berclaz, T.; Diolot, J.; Geoffroy, M.; Ginet, L. *J. Phys. E* **1977**, *10*, 871.
(19) Geoffroy, M.; Reddy, M. V. V. S. *Radiat. Phys. Chem.* **1986**, *26*, 377.
(20) Haindl, E.; Hüttermann, J. *J. Magn. Reson.* **1978**, *30*, 13.
(21) Byfleet, C. R.; Chong, D. P.; Hebden, J. A.; McDowell, C. A. *J. Magn. Reson.* **1970**, *2*, 69.
(22) (a) Binkley, J. S.; Whiteside, R. A.; Krishnan, R.; Seeger, R.; De Frees, D. J.; Schlegel, H. B.; Topiol, S.; Kahn, L. R.; Pople, J. A. *QCPE* **1981**, *13*, 406. (b) Binkley, J. S.; Frisch, M. J.; De Frees, D. J.; Raghavachari, K.; Whiteside, R. A.; Schlegel, H. B.; Fluder, E. M.; Pople, J. A. GAUSSIAN 82; Carnegie-Mellon University: Pittsburg, PA, 1983.
(23) Binkley, J. S. *J. Chem. Phys.* **1976**, *64*, 5143.
(24) Fletcher, R.; Powell, M. J. D. *Comput. J.* **1973**, *6*, 163.
(25) Mezey, P. G.; Lien, M. H.; Yates, K.; Csizmadia, G. *Theor. Chim. Acta* **1980**, *40*, 75.
(26) (a) Amos, T.; Snyder, L. C. *J. Chem. Phys.* **1964**, *41*, 1773. (b) Cremaschi, P.; Gamba, A.; Morosi, G.; Simonetta, M. *Theor. Chim. Acta* **1976**, *41*, 177.
(27) Kern, C. W.; Karplus, M. *J. Chem. Phys.* **1965**, *42*, 1062.
(28) Neumann, D. B.; Basch, H.; Kornegay, R. L.; Snyder, L. C. *QCPE*, **1971**, Program 199.

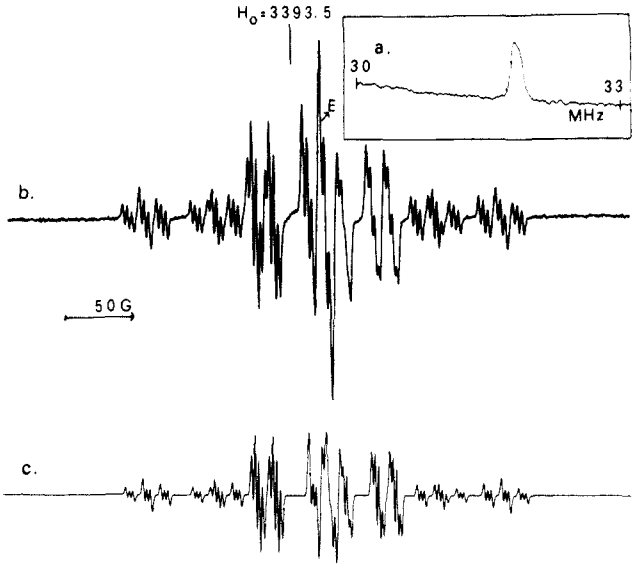

Figure 1. ESR and ENDOR spectra of the room-temperature stable radical. The magnetic field is aligned along the crystallographic *b* axis: (a) ^{1}H ENDOR spectrum obtained at the field setting indicated by E on the corresponding ESR spectrum; (b) experimental ESR spectrum indicating the presence of both allowed (weak lateral lines) and forbidden (intense central lines) transitions; (c) simulated ESR spectrum obtained by using the tensors given in Table II and a line-width parameter Γ = 2.7 G.

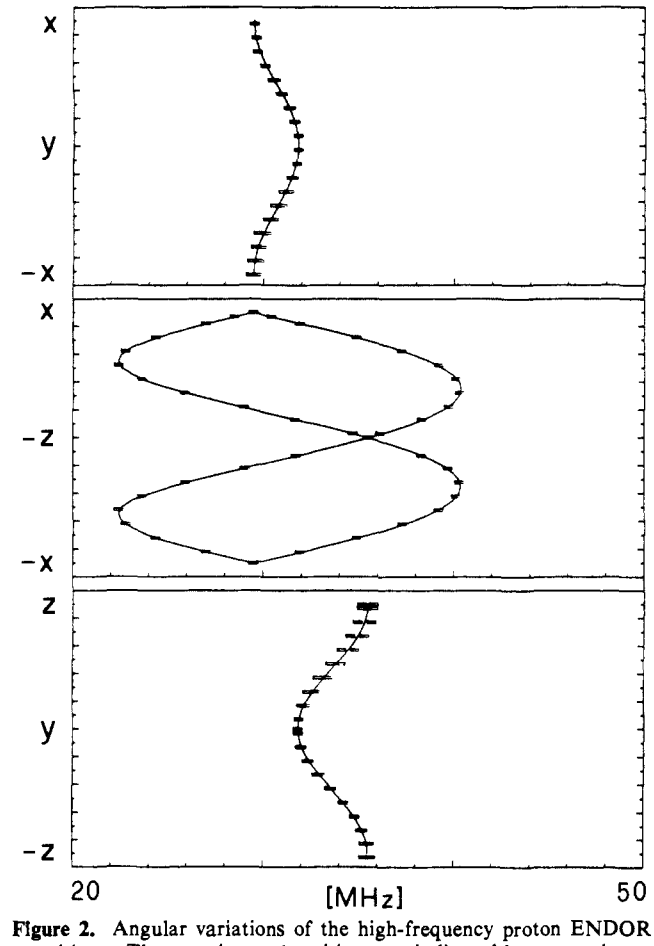

Figure 2. Angular variations of the high-frequency proton ENDOR transitions. The experimental positions are indicated by rectangles.

is the object of the present study.

An example of an ^{1}H ENDOR spectrum obtained with a crystal irradiated at room temperature is also shown in Figure 1, and the angular dependence of the corresponding signals is shown in Figure 2. The analysis of these curves is straightforward: the trapped

Table II. Experimental ESR Tensors for Radical **1**

eigenvalues	eigenvectors			magnetic or quadrupolar coupling
g tensor				
g_1 = 2.0094	0.928	0.000	−0.373	
g_2 = 2.0017	0.000	1.000	0.000	
g_3 = 2.0193	0.373	0.000	0.928	
^{1}H T (MHz)				A_{iso} = −35.6
T_1 = −17.3	0.820	0.000	0.572	τ_1 = 18.3
T_2 = −36.2	0.000	1.000	0.000	τ_2 = −0.6
T_3 = −53.3	−0.572	0.000	0.820	τ_3 = −17.7
^{79}Br T (MHz)				A_{iso} = 71.3
T_1 = 33	1.000	0.000	0.000	τ_1 = −38.3
T_2 = 131	0.000	1.000	0.000	τ_2 = 59.7
T_3 = 50	0.000	0.000	1.000	τ_3 = −21.3
^{79}Br P (MHz)				
P_1 = −54.5	1.000	0.000	0.000	e^2Qq_1 = −327
P_2 = −42.5	0.000	1.000	0.000	e^2Qq_2 = −255
P_3 = 97.0	0.000	0.000	1.000	e^2Qq_3 = 582
^{81}Br T (MHz)				A_{iso} = 76.9
T_1 = 35.6	1.000	0.000	0.000	τ_1 = −41.3
T_2 = 141.2	0.000	1.000	0.000	τ_2 = 64.3
T_3 = 53.9	0.000	0.000	1.000	τ_3 = −23.0
^{81}Br P (MHz)				
P_1 = −45.4	1.000	0.000	0.000	e^2Qq_1 = −272
P_2 = −35.4	0.000	1.000	0.000	e^2Qq_2 = −212
P_3 = 80.8	0.000	0.000	1.000	e^2Qq_3 = 484

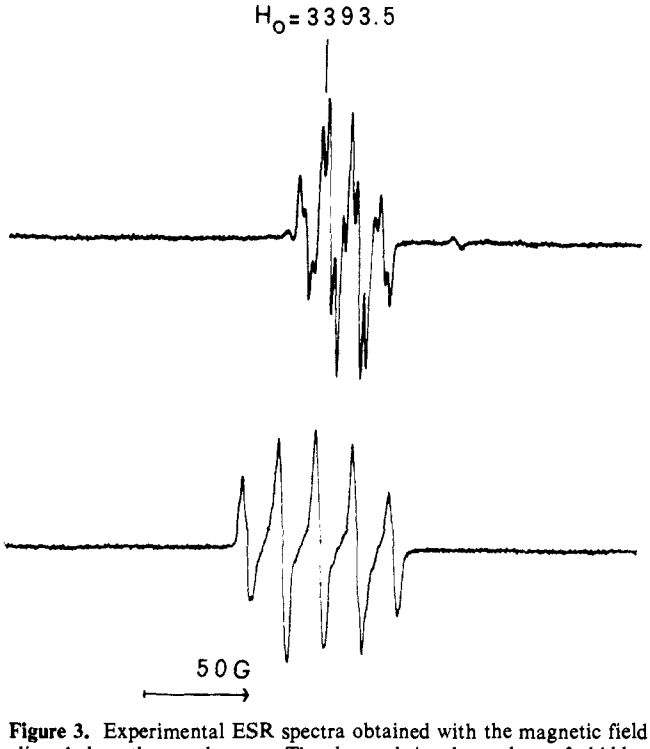

Figure 3. Experimental ESR spectra obtained with the magnetic field aligned along the *a* and *c* axes. The observed signals are due to forbidden transitions.

radical exhibits hyperfine coupling with a single proton and, as expected for an orthorhombic system, only two sites should be distinct in the crystallographic planes. The equivalence of all the sites in planes *ab* and *bc* indicate that one eigenvector is aligned along the *b* axis. The proton hyperfine tensor is given in Table II.

The angular dependence of the ESR signals is totally unsuitable for a classical analysis; the signal intensities as well as the spread of the spectrum change suddenly for many orientations, and the various transitions cannot be directly assigned. Such a behavior is undoubtedly due to the presence of nuclei exhibiting a large quadrupolar interaction. The bromine hyperfine tensors have

Table III. Optimized Parameters for Allyl and Azaallyl Radicals

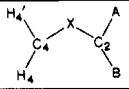

	3	4	5	5′	6
energy (ua)	−116.46809	−132.45710	−591.35900	−591.36238	−2698.10605
$\angle C_2XC_4$	124.54	119.08	118.89	124.23	118.74
$\angle AC_2B$	117.41	118.76	114.51	113.37	113.99
$\angle H_4C_4H_4$	117.41	118.76	119.03	119.23	119.10
X–C_2 (Å)	1.3904	1.3216	1.3039	1.2995	1.2993
X–C_4 (Å)	1.3904	1.3216	1.3250	1.3217	1.3245
C_2–A (Å)	1.0741	1.0736	1.7223	1.0694	1.8656
C_2–B (Å)	1.0757	1.0813	1.0759	1.7468	1.0748
C_4–H_4' (Å)	1.0741	1.0736	1.0714	1.0719	1.0716
C_4–H_4 (Å)	1.0757	1.0813	1.0811	1.0767	1.0806

therefore been obtained by using the method described above: the diagonal elements of the tensors **g**, $^{79/81}$Br-**T** and $^{79/81}$Br-**P** are deduced from the spectra obtained for H_0 along the crystallographic axes (Figures 1 and 3). These tensors allow us to simulate any spectrum recorded for H_0 oriented in the *ab* and *bc* planes. Additional elements are, however, necessary for the simulation of the spectra obtained when H_0 lies in the *ac* plane; in this plane two crystallographic sites are magnetically distinct and we have found that, besides a nondiagonal term for the proton tensor, it is necessary to include a nondiagonal *g* element (g_{xy}) in order to have a good fit between simulated and experimental spectra.[29] The hyperfine coupling with a ^{14}N nucleus has been taken into account to get the final simulated spectra. This splitting is maximum (≃3 G) along the *Y* direction. The various ESR tensors are reported in Table II together with the experimental quadrupolar coupling constants e^2Qq. It can be noticed that all these tensors have an eigenvector aligned along the *b* direction and that the Br hyperfine tensors are not involved in any site splitting. These facts are obviously due to the particular orientation of the molecule in the crystal lattice (molecular plane in the *ac* plane, C–Br bond almost aligned along the *c* axis). It is probable that the analysis of the present species has only been possible because of this exceptional crystallographic situation.

Calculations

Allyl and Azaallyl Radicals. We have first optimized the structures of the allyl **3** and azaallyl **4** radicals. The predicted structure of **3** is in very good agreement with previous calculations.[2,30] After spin annihilation of the quartet contamination,

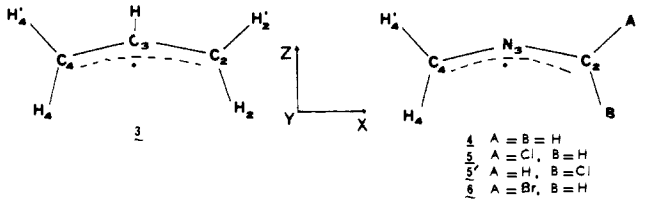

the $\langle S^2 \rangle$ values reported in Table IV are close to 0.750, which means that the spin densities obtained in this model may be used in the subsequent discussion.

Chloro- and Bromoazaallyl Radicals. The optimized structures of $CH_2{=}N{-}CHCl$ have been calculated for both the isomers exo **5** and endo **5′**. For $CH_2{=}N{-}CHBr$ the structure has been optimized only for the exo isomer **6**. The geometrical parameters are presented in Table III, whereas final (after spin annihilation) $\langle S^2 \rangle$ values together with the spin densities are given in Table IV. The components of the quadrupolar interaction with the halogen nucleus are reported in Table V together with the isotropic coupling constants.

Radical Resulting from Hydrogen Addition on a Thiazole Ring: 7 and 8. In order to estimate the influence of the incorporation of the radical inside the ring as well as that of the presence of an α-sulfur atom on the spin populations, we have calculated the spin densities for the compounds **7** and **8** (Table IV). Because

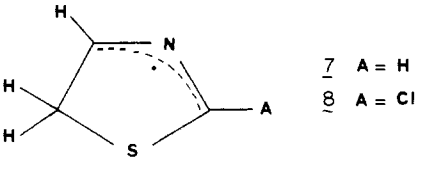

of the size of these molecules, the structures have not been optimized, but the geometries predicted for **3** and **5** have been used for **7** and **8**. The spin densities and hyperfine interaction parameters of these two radicals are given in Tables IV and V, respectively.

Table IV. Theoretical Spin Densities, after Spin Annihilation, in the Valence Orbitals for Allyl and Azaallyl Radicals[a]

radical	$\langle S^2 \rangle$	atom	net spin density	gross spin densities			
				ρ_s	ρ_x	ρ_y	ρ_z
3	0.758	C3	−0.236	−0.042	−0.032	−0.162	−0.020
		C2,C4	0.714	0.050	0.021	0.575	0.021
4	0.758	N3	−0.204	−0.023	−0.028	−0.156	−0.009
		C2,C4	0.706	0.047	0.016	0.572	0.018
5	0.758	N3	−0.202	−0.022	−0.027	−0.152	−0.008
		C2	0.701	0.043	0.015	0.516	0.016
		C4	0.725	0.048	0.016	0.589	0.019
		Cl	0.074	0.001	−0.017	0.030	−0.004
6	0.759	N3	−0.200	−0.022	−0.028	−0.152	−0.008
		C2	0.710	0.043	0.017	0.519	0.018
		C4	0.723	0.048	0.016	0.589	0.019
		Br	0.063	0.002	−0.020	0.030	0.005
7	0.757	N3	−0.191	−0.022	−0.013	−0.138	−0.019
		C2	0.677	0.038	0.013	0.473	0.015
		C4	0.702	0.045	0.016	0.511	0.016
		S	0.271	0.004	−0.008	0.089	0.001
8	0.758	N3	−0.194	−0.023	−0.013	−0.138	−0.019
		C2	0.711	0.038	0.014	0.452	0.015
		C4	0.698	0.045	0.015	0.510	0.016
		S	0.261	−0.005	−0.008	0.087	0.000
		Cl	0.060	0.002	0.000	0.025	−0.219

[a] The reference frame is given in Figure 4.

Discussion

Equilibrium Geometries. It is seen in Table III that the main difference between the optimized structure of the allyl radical and that of the azaallyl radical lies in the decrease of the CXC bond angle which passes from 124.5° for $CH_2{=}CH{-}CH_2$ to 119.0° for $CH_2{=}N{-}CH_2$. As expected, the azaallyl radical is planar and the C–N distance (1.32 Å) is shorter than a single C–N bond (experimental value for $CH_3{-}NH_2$: C–N, 1.47 Å).[31] The calculated spin densities of the azaallyl are almost identical with those of the allyl radical: 57% in the p_y orbital of each terminal carbon, −15% in the p_y orbital of the central atom. When the azaallyl radical is incorporated in the sulfur-containing ring **7**, a rather

(29) Some additional experimental and simulated spectra are available as supplementary material.

(30) Whiteside, R. A.; Frisch, M. J.; Binkley, J. S.; De Frees, D. J.; Schlegel, H. B.; Raghavachari, K.; Pople, J. A. Quantum Chemistry Archive, Carnegie-Mellon University: Pittsburg, PA, 1981.

(31) Lide, D. R. *J. Chem. Phys.* **1957**, *27*, 343.

Table V. Calculated Hyperfine Interactions[a]

	4	5	5′	6	7	8
A_{iso} (MHz)	H_A: −44.2 H_B: −33.4	H_B: −34.4 H_4': −36.7 H_4: −33.8 ^{35}Cl: 3.4	H_A: −36.7 H_4': −36.1 H_4: −31.2 ^{35}Cl: 3.0	H_B: −33.9 H_4': −36.6 H_4: −33.8 ^{79}Br: 35.3	H_2: −33.6 H_4: −37.3	H_4: −37.8 ^{35}Cl: 3.6
quadrupole interaction (halogen), MHz		e^2Qq_i = −64.9 e^2Qq_j = 28.7 e^2Qq_k = 36.3		e^2Qq_i = 589 e^2Qq_j = −269 e^2Qq_k = −319		e^2Qq_i = −70.6 e^2Qq_j = 33.2 e^2Qq_k = 37.4

[a] i, j, k is the reference frame which diagonalizes the electric field gradient: i is found to be aligned along the C-halogen bond direction; j is perpendicular to the molecular plane; halogen nucleus, ^{35}Cl or ^{79}Br.

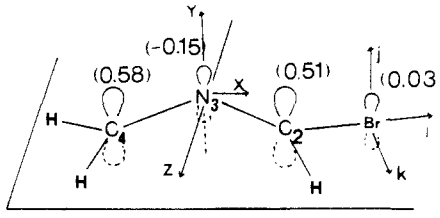

Figure 4. Calculated structure (ab initio) of the bromoazaallyl radical (the numbers in parentheses correspond to calculated densities in p_y orbitals).

high net spin density appears on the sulfur atom (Table IV). However, this spin density is strongly reduced by negative contributions from the overlap regions and, finally, the gross spin density in the $3p_y$ sulfur orbital is only 0.08. The spin populations for the azaallylic moiety in **7** are very similar to those calculated for **4** and, as illustrated by the theoretical isotropic constants A_{iso}(H′2) and A_{iso}(H′4) found for **7** and **4**, in both the cases, the unpaired electron is practically equally shared between C(2) and C(4) (Table V).

The two isomers of the chloroazaallyl radical (**5** and **5′**) present appreciable difference in the CNC geometry: the endo structure is the more stable (ΔE = 0.00289 au), and it is characterized by a smaller bending than the exo form ($\Delta\theta$ = 5.18°). Nevertheless, these two isomers do not exhibit large variations in their spin densities.[32] When the chloroazaallyl radical **5** is incorporated within a ring so as to give **8**, no drastic modification of the electronic structure of the azaallyl fragment is observed; the isotropic ^{1}H and ^{35}Cl magnetic coupling constants as well as the quadrupolar tensor remain indeed almost unchanged (Table V). The bromine species **6** presents the same features as the chlorine radical **5** ($\angle$CNC = 118.7°), and it appears, from the gross orbital populations, that the major contribution to the Br spin density is also due to the Br p_y orbital (Br p_y = 0.030). An illustration of the theoretical bromoazaallyl structure is given in Figure 4.

Calculated and Experimental Hyperfine Interactions of Bromoazaallyl. Let us now examine whether the experimental ESR/ENDOR tensors reported in Table II are consistent with the calculated spin densities of Figure 4. In Table II the magnetic hyperfine tensors are decomposed into isotropic and anisotropic coupling constants. The values obtained for the proton are consistent with an hydrogen nucleus located in α from a $2p_\pi$ unpaired electron. The measured ^{1}H A_{iso} value used in conjunction with a McConnell constant of −22.5G[33] leads to a spin density of 0.56 in the carbon p_π orbital, which is in agreement with the calculated value. Actually, the A_{iso} value for the proton H(4) is very close to the experimental value ($A_{iso,exptl}$ = −35.6 MHz, $A_{iso,calcd}$ = −36.6 MHz). The experimental H τ_2 eigenvector shows that the carbon p_π orbital is aligned perpendicular to the thiazole plane and the experimental ^{1}H τ_1 eigenvector indicates that the C–H bond of the radical makes an angle of 5.6° with the crystallographic C(4)–H(4) bond direction. The ^{1}H hyperfine interaction is therefore in agreement with the values expected for an azaallyl C–H bond located in C(4) position on the thiazole ring.

The anisotropic components of the $^{79/81}$Br magnetic coupling tensors lead, after comparison with the atomic parameters given by Morton and Preston,[34] to a spin density of 0.036 in a Br 4p orbital. Moreover, the Br τ_2 eigenvector shows that this orbital is oriented perpendicular to the thiazole plane, in accordance with Figure 4. The calculated ^{79}Br isotropic constant (Fermi interaction, Table V) is equal to 35 MHz, while the experimental value is 71.3 MHz (Table II); the accord between these two values is satisfactory since the large atomic isotropic coupling constant (A_{iso}(^{79}Br) = 32070 MHz)[34] indicates that a difference of $\simeq$30 MHz corresponds to a variation of $\simeq$0.1% in the spin density. The Br magnetic couplings therefore agree with the theoretical model; however, the too weak bromine spin density prevents the Br magnetic interaction from yielding a more detailed description of the azaallyl radical.[35] The quadrupolar interaction, which is dependent upon all the electrons surrounding the Br nucleus, is more appropriate for a structural interpretation. The experimental sets of quadrupolar coupling eigenvalues reported in Table II (^{79}Br P tensor) are entirely consistent with the theoretical values (Table V). Moreover, both the experimental and the theoretical eigenvectors associated with the intermediate quadrupolar coupling constant ($e^2Qq_{2,j}$) are oriented perpendicular to the molecular plane. The calculated eigenvector associated with the largest eigenvalue is aligned along the C–Br direction, while the corresponding experimental direction makes an angle of 5.6° only with the crystallographic bond direction. This small angle is probably due to structural distorsions occurring when the hybridization of the carbon C(5) changes from sp^2 to sp^3. This change in hybridization is likely to be also at the origin of the 5° angle formed by the crystallographic C–H bond direction with the ^{1}H τ_1 eigenvector.

Due to the presence of two atoms having a large spin–orbit coupling (Br and S), the interpretation of the **g** tensor is not straightforward. Nevertheless, it can be noticed that, in accordance with structure **1**, one of the *g* eigenvectors is oriented along the p_π orbital and corresponds to a *g* value close to that of the free electron.

For an azaallyl radical the ^{14}N hyperfine coupling is expected to be very informative about the molecular structure. Unfortunately, in our case, the complexity of the spectrum (frequent overlapping of the lines) prevents us from measuring this coupling accurately for all orientations, and we could not determine the ^{14}N hyperfine tensor. Nevertheless, the observed splittings are small and consistent with a rather low spin density on the nitrogen atom. Furthermore, in accordance with structure **1**, the maximum splitting (3 G) is observed when the magnetic field is aligned perpendicular to the radical plane.[36]

Comparison with Other Allylic Systems. Although theoretical results (Table III) lead to appreciably different bond angles for the allyl and the azaallyl optimized structures, these two species

(32) For **5′** the theoretical spin densities are the following: (ρ(C4) = 0.589, ρ(N3) = −0.149, ρ(C2) = 0.5202, ρ(C1) = 0.023; the ^{35}Cl magnetic coupling constant is A_{iso} = 3.01 MHz.

(33) Carrington, A.; McLachlan, A. *D. Introduction to Magnetic Resonance*; Harper and Row: New York, 1967.

(34) Morton, J. R.; Preston, K. F. *J. Magn. Reson.* **1978**, *30*, 577.

(35) The ^{79}Br anisotropic coupling constants obtained from ab initio calculations are −16.1, 81, and −65 MHz. By using the atomic constant $2B_0$ = 1635 MHz (ref 34), the difference between experimental and calculated values for τ_{max} corresponds only to a change of 1.3% in the spin density. The mutual orientations of experimental and theoretical eigenvectors are in complete agreement.

(36) We have calculated the ^{14}N isotropic and anisotropic coupling constants. They lead to a final diagonalized tensor whose maximum value value is indeed obtained for H_0 perpendicular to the molecular plane. However, this value (~10 G) is higher than the experimental one (~3 G).

can be produced on a five-membered ring containing a sulfur atom. The species previously observed in solution by Grossi et al.[12] corresponds to **7**, where A is a methyl group. The experimental coupling constants A_{iso}(H4) = 14.7 G and A_{is3}(N) = 3.9 G are in good accordance with the values calculated for **7** from the Fermi contact interaction (A_{iso}(H4) = 13.3 G, A_{iso}(N) = 5.0 G).

In accordance with the ab initio results obtained for the allyl and azaallyl radicals, the experimental hyperfine couplings[13] obtained for radical **9** clearly show a similar isotropic coupling

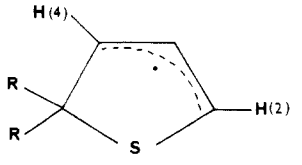

9

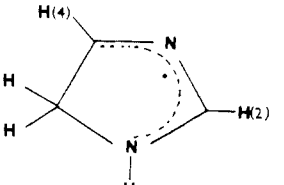

10

constant for protons H(2) and H(4). These results are in contrast with those previously reported[37,39] for the radical **10** resulting from hydrogen addition on an imidazole ring; for this latter radical the two couplings for protons H(2) and H(4) were different and the unpaired electron appeared to be delocalized onto two carbon and two nitrogen atoms.

Most of the observed heteroatoms containing allylic radicals correspond to cationic species which have been produced by ring opening of saturated small heterocycles; for example, $(CH_2-NH-CH_2)^{\bullet+}$ [7,8] and $(CH_2-O-CH_2)^{\bullet+}$ [40-42] have recently been formed by irradiation of aziridine and oxirane, respectively. These cations exhibit a ^{1}H isotropic coupling with the protons in the exo position, which is slightly higher than that found for RCH=N̈=CBrR ($CH_2-NH-CH_2^{\bullet+}$: 17 G;[7] $CH_2-O-CH_2^{\bullet+}$: 16.4 G;[40] RHC-N-CBrR$^{\bullet}$: 12.6 G), but the major difference resides in the bent structure which is more pronounced for the neutral radical (optimized structures: $CH_2-N-CH_2^{\bullet}$: 119°; $CH_2-NH-CH_2^{\bullet+}$: 127°;[9] $CH_2-O-CH_2^{\bullet+}$: 131° [3]). Unfortunately, neither the theoretical coupling tensors nor the orientations of the experimental hyperfine eigenvectors are available for these allylic cations, and further comparison would be premature.

Radiation Process

The reaction mechanism giving rise to the formation of RHC=N̈=CBrR is similar to previous observations in the thiophene series:[13] at low temperature, radical pairs are formed; they are not stable with increasing temperature and near 300 K the spectrum of an allyl-type radical is observed. This species results from the addition of a radical R on a carbon adjacent to the sulfur atom; the R fragment is, however, located too far from the allylic moiety to be identified.

Acknowledgment. We are indebted to Professor Gamba for a copy of his spin annihilation procedure within the GAUSSIAN 80 program. We thank Professor L. D. Kispert for preliminary ENDOR measurement. The financial support of the Swiss National Science Foundation is gratefully acknowledged.

Supplementary Material Available: Tables of bond lengths and angles and anisotropic displacement parameters along with a computer-generated plot, tables of form factors, and experimental and simulated ESR spectra corresponding to intermediate orientations of the magnetic field (25 pages). Ordering information is given on any current masthead page.

(37) Lamotte, B. Ph.D. Thesis, 1968, Universit de Grenoble.
(38) Westhof, E.; Flossmann, W. *J. Am. Chem. Soc.* **1975**, *97*, 6622.
(39) Kasai, P. H.; McLeod, D., Jr. *J. Am. Chem. Soc.* **1973**, *95*, 27.
(40) Snow, L. D.; Wang, J. T.; Williams, F. *Chem. Phys. Lett.* **1983**, *100*, 193.
(41) Symons, M. C. R.; Wren, B. W. *Tetrahedron Lett.* **1983**, 2315.
(42) Bally, T.; Nitsche, S.; Haselbach, E. *Helv. Chim. Acta* **1984**, *67*, 86.

A Time-Resolved ESR Study of the Kinetics of Spin Trapping by Nitromethane *aci*-Anion[1]

Keith P. Madden,* Hitoshi Taniguchi, and Richard W. Fessenden

Contribution from the Radiation Laboratory and Department of Chemistry, University of Notre Dame, Notre Dame, Indiana 46556-0768. *Received August 21, 1987*

Abstract: The kinetics of spin trapping by the *aci*-anion of nitromethane have been studied for some representative radicals in aqueous solution by using time-resolved ESR with in situ radiolysis. In nearly all cases, reaction of a radical R produced an adduct $RCH_2NO_2^-$. However, these time-resolved experiments showed that $^{\bullet}CH_2O^-$ produces both an adduct and the radical anion of nitromethane. Second-order rate constants varied from 1.4×10^7 M^{-1} s^{-1} for CO_2^- to 3.8×10^8 for the *p*-carboxyphenyl radical. Reducing radicals (CO_2^-, CH_2O^-, $(CH_3)_2COH$, and $(CH_3)_2CO^-$) react less rapidly than alkyl radicals ($CH_2CO_2^-$, CH_3) which in turn react less rapidly than σ radicals (*p*-carboxyphenyl and $CONH_2$).

Spin trapping[2,3] has greatly extended the use of electron spin resonance as a qualitative tool in the study of free-radical reactions by augmenting its intrinsic sensitivity and selectivity. In this way, ESR is provided with the ability to visualize radicals that are otherwise unobservable due to short radical lifetimes, complex hyperfine structure, or unfavorable magnetic relaxation rates. Quantitative spin trapping, dubbed "spin counting" by Janzen,[4] relies on the correlation of spin adduct ESR intensity with the initial concentration of the trapped transient radical species. The spin adduct intensity in a conventional steady-state ESR experiment (SSESR) is a reflection of spin-adduct steady-state concentration, determined by the rates of adduct formation and

(1) The research described herein was supported by the Office of Basic Energy Sciences of the Department of Energy. This is Document No. NDRL-3024 from the Notre Dame Radiation Laboratory.
(2) (a) Lagercrantz, C. *J. Phys. Chem.* **1971**, *75*, 3466-75. (b) Janzen, E. G. *Acc. Chem. Res.* **1971**, *4*, 31-40.
(3) (a) Perkins, M. J. "Spin Trapping" In *Advances in Physical Organic Chemistry*; Gold, V., Bethell, D., Eds.; Academic Press: New York, 1980; Vol. 17, pp 1-64. (b) Janzen, E. G. "A Critical Review of Spin Trapping in Biological Systems" In *Free Radicals in Biology*; Pryor, W. A., Ed.; Academic Press: New York, 1980; Vol. IV, pp 115-54.
(4) Janzen, E. G.; Evans, C. A.; Nishi, Y. *J. Am. Chem. Soc.* **1972**, *94*, 8236-8.

0002-7863/88/1510-2753$01.50/0